Dense and hot matter within the nonlinear Walecka model

A. M. S. Santos and D. P. Menezes
Departamento de Física, CFM, Universidade Federal de Santa Catarina, Florianópolis-SC, Caixa Postal 476-CEP 88.040-900, Brazil
(Received 9 December 2003; published 21 April 2004)

In this work we study the effects of temperature on the equations of state obtained within a relativistic model, with and without β equilibrium over a wide range of densities. We also compare the results of the equation of state, effective mass, and strangeness fraction for the TM1, NL3, and GL sets of parameters. We have checked that TM1 and NL3 are not appropriate for the description of neutron and protoneutron stars.

DOI: 10.1103/PhysRevC.69.045803 PACS number(s): 26.60.+c, 21.30.−x, 21.65.+f, 95.30.Tg

I. INTRODUCTION

Understanding the properties of nuclear matter at both normal and high densities is of crucial importance in explaining the appearance of protoneutron and neutron stars after the supernova explosion and the formation of transiron elements in nuclear reactions. Recent experiments with unstable nuclear beams at RIKEN and experiments with relativistic heavy ions taking place at RHIC are potential tools in determining which are the appropriate equations of state (EOS) that are able to describe hot and dense matter.

Moreover, the structure of compact stars is characterized by its mass and radius, which are obtained from appropriate EOS at densities of about one order of magnitude higher than those observed in ordinary nuclei. EOS can be derived either from relativistic or potential models. The latter ones are normally developed within a nonrelativistic formalism [1] and some of them include also a three-body force [2,3] in order to solve the causality problem and to improve the description of the symmetry energy. We have opted to work with relativistic models and hence it is important to check the validity of these models at finite temperature and different densities, ranging from normal nuclear saturation density up to ten times this value.

In Ref. [4], the authors have investigated EOS with arbitrary fixed proton fractions at finite temperature and also with the inclusion of β equilibrium in order to provide appropriate EOS for supernova explosions and neutron stars. The authors have claimed that the TM1 [4] parameter set is a good choice because it reproduces the available data of stable and unstable nuclei and, in addition, yields an equation of state within a mean field approach which is similar to the one obtained with the relativistic Brueckner-Hartree-Fock theory [5]. Note that TM1 requires a nonlinear ω term in the Lagrangian density.

In this work we obtain the EOS for dense and hot matter with three different parameter sets of the nonlinear Walecka model (NLWM) [6,7], namely, TM1 [4], NL3 [8], and GL [9]. The first two have been proposed to describe nuclei ground-state properties, and the GL parametrization was proposed to describe the equation of state of neutron stars. We have opted to use these three sets of parameters because they are widely used in the recent literature. We first fix the proton fractions and consider only matter with protons and neutrons, in the same spirit as Ref. [4]. Then we include the baryonic octet and the lightest leptons in our Lagrangian density and consider them in chemical equilibrium in neutral matter as in Ref. [10]. We work in the framework of the NLWM [6], where hadrons are coupled to scalar-isoscalar ϕ, vector-isoscalar V^μ, and vector-isovector $\vec{b}^\mu$ meson fields. Temperature effects are taken into account by including the Thomas-Fermi distribution function in the EOS. We have studied the EOS up to 20 MeV based on the temperature expected in the interior of protoneutron stars, which is, at most, 30 MeV [11]. The obtained EOS are then used in solving the Tolman-Oppenheimer-Volkoff (TOV) [12] differential equations in order to calculate the compact star properties. The best choice for the parameter set is discussed.

II. THE NLWM WITHIN THE THOMAS-FERMI APPROXIMATION AT FINITE TEMPERATURE

The Lagrangian density used in this work reads

$$\mathcal{L} = \mathcal{L}_{nucleons} + \mathcal{L}_{mesons}, \tag{1}$$

where

$$\mathcal{L}_{nucleons} = \bar{\psi}\left[\gamma_\mu\left(i\partial^\mu - g_v V^\mu - \frac{g_\rho}{2}\vec{\tau}\cdot\mathbf{b}^\mu\right) - M^*\right]\psi, \tag{2}$$

$$\mathcal{L}_{mesons} = \frac{1}{2}(\partial_\mu\phi\partial^\mu\phi - m_s^2\phi^2) - \frac{1}{3!}\kappa\phi^3 - \frac{1}{4!}\lambda\phi^4 - \frac{1}{4}\Omega_{\mu\nu}\Omega^{\mu\nu} + \frac{1}{2}m_v^2(V_\mu V^\mu)^2 + \frac{1}{4!}\xi g_v^4(V_\mu V^\mu)^2 - \frac{1}{4}\mathbf{B}_{\mu\nu}\cdot\mathbf{B}^{\mu\nu} + \frac{1}{2}m_\rho^2\mathbf{b}_\mu\cdot\mathbf{b}^\mu \tag{3}$$

with

$$\Omega_{\mu\nu} = \partial_\mu V_\nu - \partial_\nu V_\mu, \tag{4}$$

$$\mathbf{B}_{\mu\nu} = \partial_\mu\mathbf{b}_\nu - \partial_\nu\mathbf{b}_\mu - g_\rho(\mathbf{b}_\mu\times\mathbf{b}_\nu), \tag{5}$$

where $\vec{\tau}$ is the isospin operator; g_v, g_ρ, and g_s are the coupling constants of the nucleons to the mesons; $M^* = M - g_S\phi$ is the effective mass of the nucleons; m_s, m_v, and m_ρ are the masses of the mesons; and κ, λ, and ξ are the self-interaction coupling constants, provided by the sets of parameters we use in this work. The values of the parameters and the result-

TABLE I. Parameter sets used in this work. All masses are given in MeV.

Force	M	m_s	m_v	m_ρ	g_s	g_v	g_ρ	κ/M	λ	ξ
TM1	938.0	511.198	783.0	770.0	10.0289	12.6139	9.2644	3.04	3.7098	0.0169
NL3	939.0	508.194	782.501	763.0	10.217	12.868	8.948	4.377	−173.31	0.0
GL	938.0	511.198	783.0	770.0	8.188	9.197	9.732	4.546	193.110	0.0

ing bulk properties are displayed in Tables I and II, respectively. From the Euler-Lagrange formalism we obtain the equations of motion for the nucleons and for the meson fields. By replacing the meson fields by their mean values:

$$\langle\phi\rangle \equiv \langle\phi\rangle = \phi_0,$$

$$\langle V^0\rangle \equiv \langle V^0\rangle = V_0,$$

$$\langle b^0\rangle \equiv \langle b^0\rangle = b_0,$$

the equations of motion read

$$\phi_0 = -\frac{k}{2m_s^2}\phi_0^2 - \frac{\lambda}{6m_s^2}\phi_0^3 + \frac{g_s}{m_s^2}\rho_s,$$

$$V_0 = -\frac{\xi}{6m_v^2}g_v^4(V_0)^3 + \frac{g_v}{m_v^2}\rho_B,$$

$$\mathbf{b}_0 = \frac{g_\rho}{2m_\rho^2}\rho_3, \tag{6}$$

where

$$\rho_s = \gamma\sum_{i=p,n}\frac{1}{\pi^2}\int p^2 dp\frac{M^*}{\epsilon}(f_{i+}+f_{i-}),$$

$$\rho_i = \frac{1}{\pi^2}\int p^2 dp(f_{i+}-f_{i-}) \quad (i=p,n) \tag{7}$$

and ρ_B and ρ_3 are defined as $\rho_B=\rho_p+\rho_n$ and $\rho_3=\rho_p-\rho_n$; γ is the isospin degeneracy and $f_{i\pm}$ is the distribution function for particles and antiparticles, respectively, whose expression will be shown later.

In order to treat the system as a Fermi gas, one needs to work with the thermodynamic potential, which is defined as

TABLE II. Nuclear matter properties for the parameter sets used in this work.

	NL3 [8]	TM1 [4]	GL [9]
B/A	16.3	16.3	15.95
$\rho_0(\mathrm{fm}^{-3})$	0.148	0.145	0.145
K(MeV)	272	281	285
$\mathcal{E}_{sym.}$(MeV)	37.4	36.9	36.8
M^*/M	0.6	0.63	0.77

$$\Omega = E - TS - \sum_{i=p,n}\mu_i N_i, \tag{8}$$

where μ_i is the chemical potential of nucleon i, N_i is the baryon number of nucleon i:

$$N_i = \int d^3r\rho_i, \tag{9}$$

and S is the classical entropy of the Fermi gas, which is given by

$$S = -\gamma\sum_{i=p,n}\int\frac{d^3rd^3p}{(2\pi)^3}\left[f_{i+}\left(\frac{f_{i+}}{1-f_{i+}}\right) + \ln(1-f_{i+}) + (f_{i+}\leftrightarrow f_{i-})\right]. \tag{10}$$

The expression of the thermodynamical potential in the Thomas-Fermi approximation (TFA) (for a more detailed calculation please refer to Ref. [13]) becomes

$$\Omega = \int d^3r\left(\frac{1}{2}[(\boldsymbol{\nabla}\phi)^2 - (\boldsymbol{\nabla}V_0)^2 - (\boldsymbol{\nabla}b_0)^2] - V_{ef}\right), \tag{11}$$

with

$$V_{ef} = -\frac{1}{2}\left[m_s^2\phi^2 + \frac{2}{3!}\kappa\phi^3 + \frac{2}{4!}\lambda\phi^4 - m_v^2V_0^2 - \frac{2}{4!}\xi g_v^4V_0^4 - m_\rho^2b_0^2\right] + \gamma T\sum_i\int\frac{d^3p}{2\pi^2}[\ln(1+e^{-(\epsilon-\nu_i)/T}) + \ln(1+e^{-(\epsilon-\nu_i)/T})]. \tag{12}$$

In the static, homogeneous nuclear matter assumption we have made, the terms ϵ and ν_i are given, respectively, by $\epsilon = \sqrt{p^2+M^{*2}}$ and $\nu_{i0}=\mu_i-g_vV_0-g_\rho\tau_3b_0$, where τ_3 is the appropriate isospin projector for the baryon charge states.

As mentioned above, temperature effects are considered here by introducing the Thomas-Fermi approximation, where particles and antiparticles contribute for the energy of the system. For a system in equilibrium, the thermodynamical potential is stationary.We can therefore minimize it with respect to the distribution functions, leaving fixed the meson fields:

$$\left.\frac{\partial\Omega}{\partial f_{i+}}\right|_{f_{i-},f_{j\pm},\phi_0,V_0,b_0} = 0, \quad i\neq j, \tag{13}$$

which leads to

$$f_{i\pm} = \frac{1}{1+e^{[(\epsilon\mp\nu_{i0})/T]}}. \tag{14}$$

In the TFA, the energy density and the pressure are, therefore,

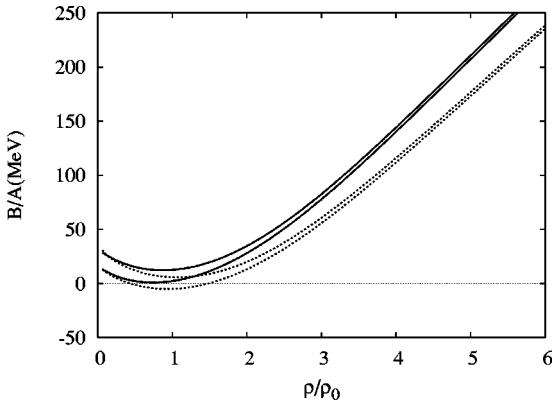

FIG. 1. Binding energy versus relative baryonic density at different temperatures: $Y_p=0.2$ (solid curves) and $Y_p=0.3$ (dotted ones). The couple of curves reaching higher values stand for the EOS at 20 MeV; lower ones for EOS at 10 MeV. The TM1 set has been used here.

$$\mathcal{E}=\frac{\gamma}{2\pi^2}\sum_{i=p,n}\int p^2dp\sqrt{p^2+M^{*2}}(f_{i+}+f_{i-})+\frac{m_v^2}{2}V_0^2 + \frac{1}{8}\xi g_v^4(V_0)^4+\frac{m_\rho^2}{2}b_0^2+\frac{m_s^2}{2}\phi_0^2+\frac{\kappa}{6}\phi_0^3+\frac{\lambda}{24}\phi_0^4 \quad (15)$$

and

$$P=\frac{\gamma}{6\pi^2}\sum_{i=p,n}\int\frac{p^4dp}{\sqrt{p^2+M^{*2}}}(f_{i+}+f_{i-})+\frac{m_v^2}{2}V_0^2+\frac{1}{24}\xi g_v^4(V_0)^4 + \frac{m_\rho^2}{2}b_0^2-\frac{m_s^2}{2}\phi_0^2-\frac{k}{6}\phi_0^3-\frac{\lambda}{24}\phi_0^4. \quad (16)$$

III. INCLUDING THE BARYONS OF THE OCTET

In this section we include the eight lightest baryons and the lightest leptons in our treatment, as they are expected to be found at large values of density and temperature. The Lagrangian density with the baryonic octet reads

$$\mathcal{L}=\sum_B\overline{\psi_B}\left[\gamma_\mu\left(i\partial^\mu-g_{vB}V^\mu-\frac{g_{\rho B}}{2}\vec{\tau}\cdot\mathbf{b}^\mu\right)-M_B^*\right]\psi_B + \frac{1}{2}(\partial_\mu\phi\partial^\mu\phi-m_s^2\phi^2)-\frac{1}{3!}\kappa\phi^3-\frac{1}{4!}\lambda\phi^4-\frac{1}{4}\Omega_{\mu\nu}\Omega^{\mu\nu} + \frac{1}{2}m_v^2V_\mu V^\mu+\frac{1}{4!}\xi g_v^4(V_\mu V^\mu)^2-\frac{1}{4}\mathbf{B}_{\mu\nu}\cdot\mathbf{B}^{\mu\nu} + \frac{1}{2}m_\rho^2\mathbf{b}_\mu\cdot\mathbf{b}^\mu+\sum_{l=e^-,\mu^-}\overline{\psi_l}(i\gamma_\mu\partial^\mu-m_l)\psi_l, \quad (17)$$

where $g_{vB}=\chi_{vB}g_v$, $g_{\rho B}=\chi_{\rho B}g_\rho$, and $g_{sB}=\chi_{sB}g_s$ are the coupling constants of baryon "B" to the mesons. We use the nucleon to meson couplings equal to 1 and the hyperon to meson couplings equal to $\sqrt{2/3}$ as suggested in Refs. [11,14] throughout this work. This choice is based on quark counting arguments. There are other choices based on more sophisticated features [11,15], where the hyperon coupling constants are constrained by the binding of the Λ hyperon in nuclear matter, hypernuclear levels, and neutron star masses and the couplings to the Σ and Ξ are assumed to be equal to those of the Λ hyperon. However, we are mainly interested in verifying the effects of the parameters which play a primary role in describing nuclear matter. For this reason we have used just one of the possible hyperon-meson coupling constants.

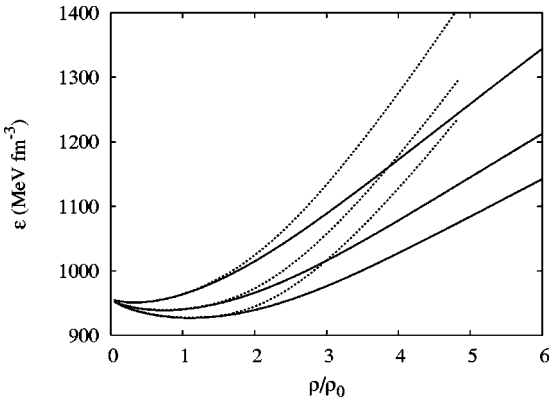

FIG. 2. Energy density curves for relative baryonic density in the NLWM at 10 MeV, with the TM1 and NL3 parameter sets. From top to bottom: $Y_p=0.0$, 0.3, and 0.5. The dotted curves have been obtained with NL3 and solid ones with TM1.

$M_B^*=M_B-g_{sB}\phi$, where M_B is the mass of baryon B and m_v, m_ρ, and m_s are the masses of the mesons. The equations of motion in this case read

$$\phi_0=-\frac{k}{2m_s^2}\phi_0^2-\frac{\lambda}{6m_s^2}\phi_0^3+\sum_B\frac{g_s}{m_s^2}\chi_{sB}\rho_{sB},$$

$$V_0=-\frac{\xi}{6m_v^2}g_v^4(V_0)^3+\sum_B\frac{g_v}{m_v^2}\chi_{vB}\rho_B,$$

$$\mathbf{b}_0=\sum_B\frac{g_\rho}{m_\rho^2}\chi_{\rho B}\tau_{3B}\rho_B, \quad (18)$$

where

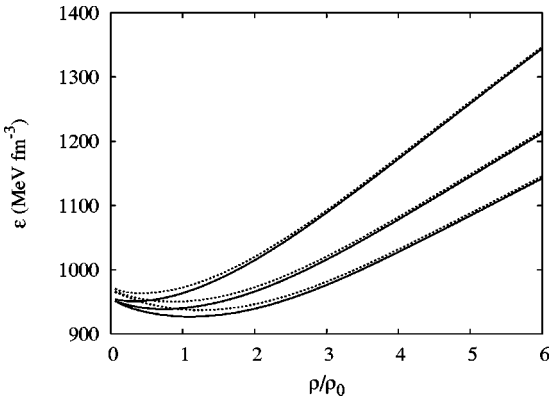

FIG. 3. Energy density curves in the NLWM at $T=10$ (solid line) and $T=20$ MeV (dashed), with the TM1 parameter set for different proton fractions. From top to bottom: $Y_p=0.0$, 0.3, and 0.5.

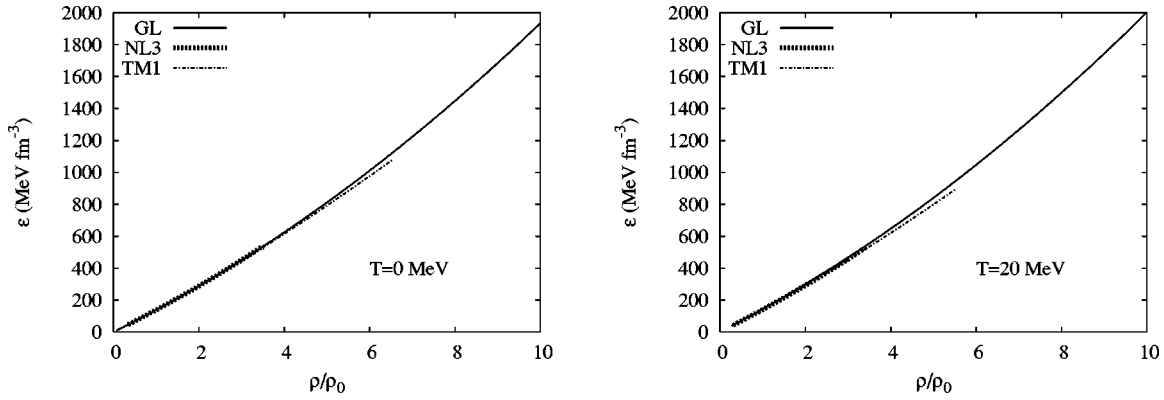

FIG. 4. Energy density in the NLWM in the presence of the octet at different temperature values, with different parameter sets.

$$\rho_{sB} = \frac{1}{\pi^2}\int p^2 dp \frac{M_B^*}{\epsilon_B}(f_{B+} + f_{B-}),$$

$$\rho_B = \frac{1}{\pi^2}\int p^2 dp (f_{B+} - f_{B-}).$$

The distribution function for the baryons is

$$f_{B\pm} = \frac{1}{1 + e^{[(\epsilon_B \mp \nu_{B0})/T]}}, \tag{19}$$

where ϵ_B and ν_{B0} are given, respectively, by

$$\epsilon_B = \sqrt{p^2 + M_B^{*2}}$$

and

$$\nu_{B0} = \mu_B - g_{\nu B} V_0 - g_{\rho B}\tau_{3B} b_0.$$

As discussed above, the star is treated here in its equilibrium era, i.e., the system is considered to have attained a stage where decays are forbidden. After the deleptonization takes place, the entropy is maximum and the temperature increases again, as shown in Ref. [17] where mixed and quark phases have also been considered. If only hadrons are considered, the temperatures can be even higher. Since the system has already been deleptonized, the neutrino chemical potentials are zero. Hence, we have $\mu_{\nu_{e^-}} = \mu_{\nu_{\mu^-}} = 0$ and

$$\mu_{\Sigma^0} = \mu_{\Xi^0} = \mu_\Lambda = \mu_n,$$

$$\mu_{\Sigma^-} = \mu_{\Xi^-} = \mu_{n+}\mu_{e^-},$$

$$\mu_{\Sigma^+} = \mu_p = \mu_n - \mu_{e^-},$$

$$\mu_\mu = \mu_e. \tag{20}$$

The expressions for the energy density and the pressure in this model at finite temperature read

$$\mathcal{E} = \frac{1}{\pi^2}\sum_B \int p^2 dp \sqrt{p^2 + M_B^{*2}}(f_{B+} + f_{B-}) + \frac{1}{\pi^2}\sum_l \int p^2 dp \sqrt{p^2 + m_l^2}(f_{l-} + f_{l+}) + \frac{m_v^2}{2}V_0^2 + \frac{\xi g_v^4}{8}V_0^4 + \frac{m_\rho^2}{2}b_0^2 + \frac{m_s^2}{2}\phi_0^2 + \frac{\kappa}{6}\phi_0^3 + \frac{\lambda}{24}\phi_0^4 \tag{21}$$

and

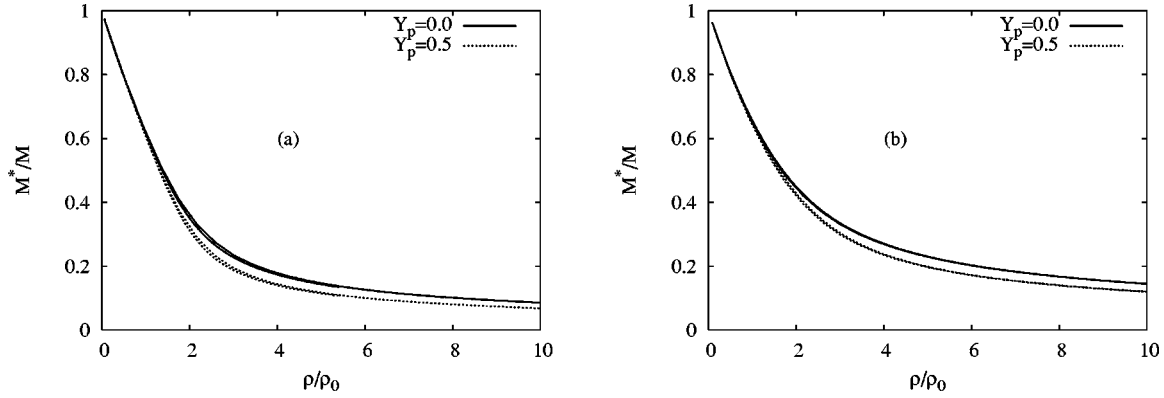

FIG. 5. Effective mass curves for nucleons in the model with different proton fractions: $Y_p = 0.0$ and $Y_p = 0.5$, with parametrizations NL3 (a), and TM1 (b), at $T = 0$ MeV (higher) and $T = 20$ MeV (lower values).

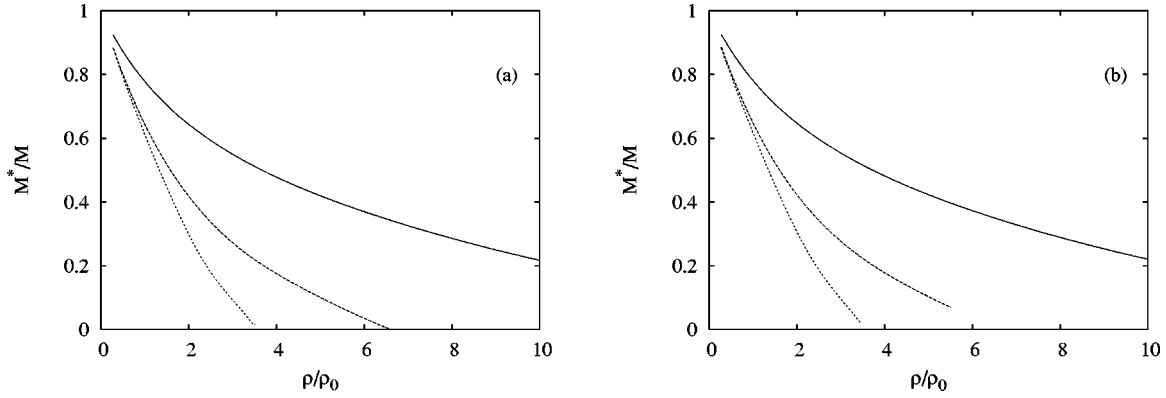

FIG. 6. Effective mass curves for nucleons in the model with the octet baryons, with parametrizations NL3 (bottom), TM1, and GL (top), at (a) $T=0$ MeV and (b) $T=20$ MeV.

$$P = \frac{\gamma}{3\pi^2}\sum_B \int \frac{p^4 dp}{\sqrt{p^2+M^{*2}}}(f_{B+}+f_{B-}) + \frac{1}{\pi^2}\sum_l \int \frac{p^4 dp}{\sqrt{p^2+m_l^2}}(f_{l-}+f_{l+}) + \frac{m_v^2}{2}V_0^2 + \frac{\xi g_v^4}{24}V_0^4 + \frac{m_\rho^2}{2}b_0^2 - \frac{m_s^2}{2}\phi_0^2 - \frac{\kappa}{6}\phi_0^3 - \frac{\lambda}{24}\phi_0^4, \quad (22)$$

where the distribution function for the leptons and antileptons are

$$f_{l\pm} = \frac{1}{1+e^{[(\epsilon_l \mp \mu_l)/T]}}, \quad (23)$$

with $\epsilon_l = \sqrt{p_l{}^2 + m_l^2}$, μ_l is the chemical potential of lepton "l," and m_l its mass ($m_e = 0.551$ MeV for the electron and $m_\mu = 106.55$ MeV for the muon).

IV. A COMPARATIVE STUDY OF THE TM1, GL, AND NL3 SETS OF PARAMETERS

In Fig. 1 we show the binding energies for two values of proton fraction ($Y_p = 0.2$ and $Y_p = 0.3$), at temperatures 10 and 20 MeV. As expected, higher values of proton fractions bring the binding energy down to lower values. We see here that temperature increase acts on star matter so as to make impossible bound states for $Y_p = 0.2$ at 10 MeV, whereas it is unbound at 20 MeV. This behavior has already been found in Ref. [16]. Although in different scales one can also compare these curves with the ones shown in Ref. [4] and verify that their trend is the same.

In Fig. 2 we plot the energy density curves for TM1 and NL3, with different proton fractions at finite temperature. We can see that NL3 makes the EOS considerably harder than TM1, as the baryonic density increases, a confirmation of what was stated in Ref. [4]. In Fig. 3 we have used TM1 to obtain the energy densities at 10 and 20 MeV. From Figs. 2 and 3 we conclude that the EOS vary more with the parametrization than with temperature, within the temperature range we have studied.

Now with the inclusion of the octet (therefore with β equilibrium), the energy density curves for the three parameter sets are shown in Fig. 4. The values are quite similar for the parameter sets, with slight hardening effects on the EOS due to temperature. Note that the NL3 and GL curves are coincident up to $3.5\rho/\rho_0$. One can also see that NL3 stops converging before TM1 which also stops converging. The reason for this fact is explained as follows. The effective mass curves for the nucleons at different proton fractions (no β equilibrium imposed), at different temperature values, are shown in Fig. 5. These figures are to be compared with the ones displayed in Fig. 6, where the octet has been considered. From the values of effective masses (with the octet baryons, β equilibrium) given in Fig. 6 we can see that they are dependent on the temperature, but strongly dependent on the parameters used. We also conclude that GL provides a satisfactory description of the nuclear matter for a wide range of densities; TM1 fails to describe the effective mass if hyperons are included, as the baryonic density comes to ~ 6.5 times the nuclear saturation density; and NL3 also fails at ~ 3.5 times the saturation density. The curves for higher temperatures are very similar as $T=0$, so we do not show them here. Note that TM1 and NL3 only fail because baryons other than protons and neutrons were included, as they do not present zero effective masses in Fig. 5. In Figs. 7 and 8 we plot the particle population of all baryons and leptons for $T=0$, 10, and 20 MeV, respectively. We can easily see that electrical neutrality is conserved: positively charged par-

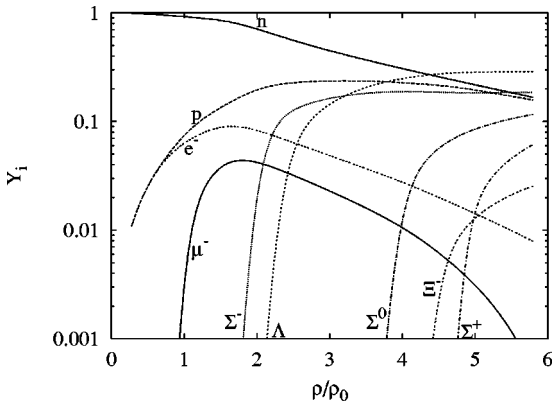

FIG. 7. Particle population $Y_i = \rho_i/\rho_B$, i= baryons and leptons at zero temperature.

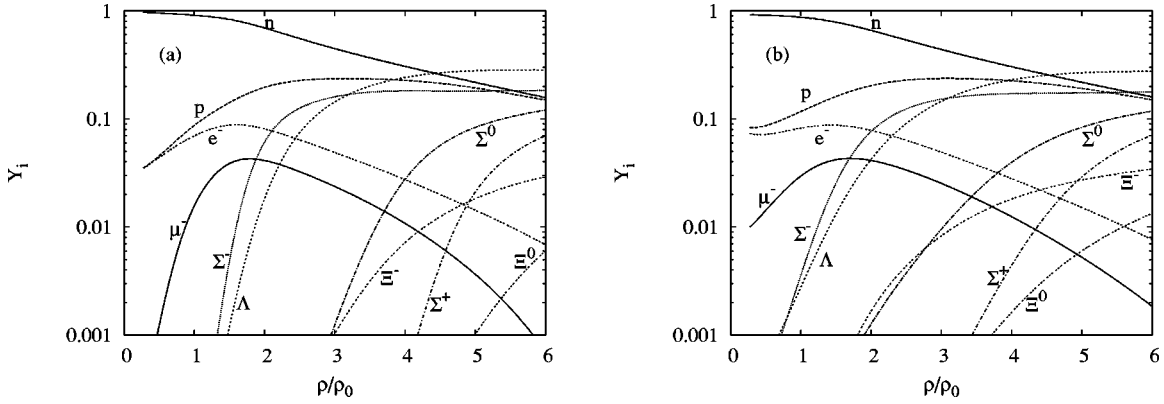

FIG. 8. The same as in Fig. 7 for (a) $T=10$ MeV, (b) $T=20$ MeV.

ticles have their population increased as negative hyperons appear. Heaviest hyperons come about at higher densities, as expected—inner regions of neutron stars are presumably populated by heavier baryons. Hyperons turn up at lower densities as temperature increases and more hyperons show up. The heaviest baryon of the octet Ξ^0 appears already at $T=10$ MeV. All plots of particle population that we show here have been obtained with the TM1 set. For densities higher than $6.5\rho/\rho_0$, only the GL parametrization can be used.

Concerning the strangeness fraction shown in Fig. 9, different parameter sets provide different results for its values. The strangeness fraction, defined in Ref. [17] among other papers, reaches almost 1/3 for the GL parametrization at $10\rho/\rho_0$ (density of the interior of a protoneutron star). TM1 and NL3 provide remarkably higher values of strangeness fraction for lower densities. For all three sets the values have a slight increase with temperature. We conclude that strangeness fractions are more sensitive to the parametrization than to temperature.

We finally discuss how different parametrizations can be used when studying warm stellar objects. The importance of such analysis lies chiefly on finding out maximum masses (or radius) of compact stars, which decides whether it remains as a star or collapses to a black hole. Spherically symmetric and static star assumptions can be made on Einstein's general relativity equations, leading to the Tolman-Oppenheimer-Volkoff equations [12], which are

$$\frac{dP}{dr} = -\frac{G}{r}\frac{[\mathcal{E}+P][M+4\pi r^3 P]}{(r-2GM)}, \tag{24}$$

$$\frac{dM}{dr} = 4\pi r^2 \mathcal{E}, \tag{25}$$

with G as the gravitational constant and $M(r)$ as the enclosed gravitational mass. We have used $c=1$. For a certain EOS at a certain temperature, the TOV equations are integrated from the origin for a set of arbitrary choices of central density, so that they define a one-parameter family of stars. The maximum mass of a neutron star, along with the energy density value in its core, as a function of central density, at different temperature values and with different parametrizations is shown in Table III. We see that the maximum mass either increases or attains a steady value with the temperature values used. It is also worth checking that our values of limiting mass are within the observed values, which lie between $1.4M_\odot$ and $1.8M_\odot$. At this point it is important to emphasize that the NL3 values were included just for the sake of comparison since the central energy of the stars are believed to be much higher than the value its EOS can provide. Moreover, the radius of the maximum mass star is sensitive to the low density EOS. For accurate results, the numbers at very low densities had to be improved. For

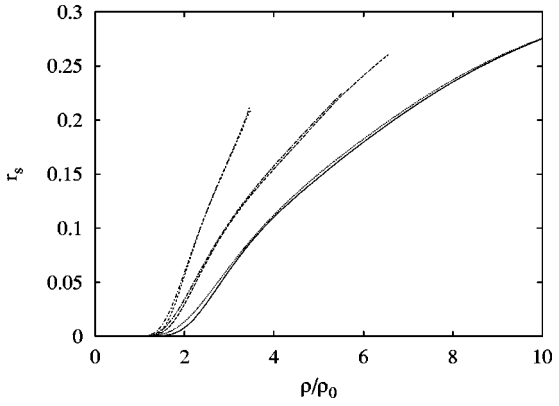

FIG. 9. Strangeness fractions at 10 and 20 MeV for the three sets of parameters. Left curves are for NL3, center ones for TM1, and right ones for GL. The lower values for each parametrization stand for the EOS in the NLWM at 10 MeV; higher values for 20 MeV.

TABLE III. Maximum masses, radius, and energy density in a neutron star sequence. Each energy density value shown above corresponds to its relevant limiting mass case.

Star profile	$M_{max}/M_\odot$			$\mathcal{E}(\mathrm{fm}^{-4})$		
Temperature (MeV)	0	10	20	0	10	20
TM1	1.37	1.40	1.40	4.99	4.29	4.47
NL3	1.31	1.32	1.39	2.42	2.48	2.48
GL	1.73	1.75	1.75	5.99	5.87	6.18

this reason we do not display the values we have obtained for the maximum radii.

V. CONCLUSION

In this work we have studied the EOS for three different parametrizations of the NLWM under two different assumptions. First of all, just protons and neutrons were considered and the proton fraction was fixed. The results were compared for different temperatures. We have checked that within the range of temperatures studied, the results vary more with different choices of the parameter than with temperature. We have then included the baryonic octet and considered a system in β equilibrium. In this case the resulting EOS could be tested by solving the TOV equations and comparing the star properties with the expected one; due to the limitations on the convergence of NL3 and TM1 parameter sets the star central energy came up lower than with the GL force. The conclusion of the present work which refers to the GL parameter set as the only choice for EOS existing at densities larger than $6.5\rho/\rho_0$ has already been used in Ref. [17], where mixed phases in the interior of hybrid stars were built.

ACKNOWLEDGMENTS

This work was partially supported by CNPq (Brazil) and CAPES (Brazil) (A.M.S.).

[1] O. Sjoberg, Nucl. Phys. **A141**, 161 (1974); J. Cugnon, P. Deneye, and A. Lejeune, Z. Phys. A **328**, 409 (1987); I. Bombaci and U. Lombardo, Phys. Rev. C **44**, 1892 (1991).
[2] R. B. Wiringa, V. Fiks, and A. Fabrocini, Phys. Rev. C **38**, 1010 (1988).
[3] W. Zuo, A. Lejeune, U. Lombardo, and J. F. Mathiot, Nucl. Phys. **A706**, 418 (2002); Eur. Phys. J. A **14**, 469 (2002).
[4] K. Sumiyoshi, H. Kuwabara, and H. Toki, Nucl. Phys. **A581**, 725 (1995).
[5] R. Brockmann and R. Machleidt, Phys. Rev. C **42**, 1965 (1990).
[6] B. D. Serot and J. D. Walecka, Adv. Nucl. Phys. **16**, 1 (1985).
[7] J. Boguta and A. R. Bodmer, Nucl. Phys. **A292**, 413 (1977).
[8] G. A. Lalazissis, J. König, and P. Ring, Phys. Rev. C **55**, 540 (1997).
[9] N. K. Glendennig, Astrophys. J. **293**, 470 (1985).
[10] A. L. Espíndola and D. P. Menezes, Phys. Rev. C **65**, 045803 (2002).
[11] N. K. Glendenning, *Compact Stars* (Springer-Verlag, New York, 2000).
[12] R. C. Tolman, Phys. Rev. **55**, 364 (1939); J. R. Oppenheimer and G. M. Volkoff, *ibid.* **55**, 374 (1939).
[13] D. P. Menezes and C. Providência, Nucl. Phys. **A650**, 283 (1999).
[14] S. A. Moszkowski, Phys. Rev. D **9**, 1613 (1974).
[15] N. K. Glendenning and S. Moszkowski, Phys. Rev. Lett. **67**, 2414 (1991).
[16] S. S. Avancini, M. E. Bracco, M. Chiapparini, and D. P. Menezes, Phys. Rev. C **67**, 024301 (2003).
[17] D. P. Menezes and C. Providência, Phys. Rev. C **68**, 035804 (2003); Phys. Rev. C (to be published).